Volumetric Testing Parallel to the Boundary Surface for a Nonconforming Discretization of the Electric-Field Integral Equation

Eduard Ubeda, Juan M. Rius, Alex Heldring, and Ivan Sekulic

***Abstract*—The volumetric monopolar-RWG discretization of the electric-field integral equation (EFIE) imposes no continuity constraint across edges in the surface discretization around a closed conductor. The current is expanded with the monopolar-RWG set and the electric field is tested over a set of tetrahedral elements attached to the boundary surface. This scheme is facet-oriented and therefore, well suited for the scattering analysis of nonconformal meshes or composite objects. The observed accuracy, though, is only competitive with respect to the RWG-discretization for a restricted range of heights of the tetrahedral elements. In this communication, we introduce a novel implementation of the volumetric monopolar-RWG discretization of the EFIE with testing over a set of wedges. We show with RCS and near-field results that this scheme offers improved accuracy for a wider range of heights than the approach with tetrahedral testing. The application of the wedge testing to the even-surface odd-volumetric monopolar-RWG discretization of the EFIE, edge-oriented and therefore less versatile, shows similar accuracy as with tetrahedral testing, which is a sign of robustness.**

***Index Terms*—Basis functions, electric-field integral equation (EFIE), integral equations, moment method.**

I. Introduction

The discretization of the electric-field integral equation (EFIE) for perfectly conducting objects is very often based on the low-order divergence-conforming RWG basis functions [1], [2]. The application of the edge-oriented RWG basis functions to composite objects, with piecewise homogeneous regions, brings out some pitfalls: 1) if the adopted mesh is conformal, the imposition of normal current continuity around junctions becomes very awkward [3], [4] and 2) if the adopted mesh is nonconformal, arising from the interconnection of triangulations with nonmatching edges, the RWG basis functions cannot be used. In these scenarios, a facet-oriented implementation of the EFIE, like the recently proposed volumetric monopolar-RWG discretization of the EFIE [5], [6], appears better suited: 1) the current is expanded with the monopolar-RWG basis functions, with no continuity across edges [7] and 2) the fields are tested over a set of tetrahedral elements attached to the surface triangulation, inside the body, to make the hyper-singular Kernel contributions numerically manageable.

In this communication, we present a new implementation of the volumetric monopolar-RWG discretization of the EFIE, so that the field testing is carried out over a set of wedges attached to the surface triangulation. Although this approach adds some complexity in the definition of the testing elements, improved accuracy is observed when compared with the tetrahedral testing for a wider range of heights of the testing elements. The testing over wedges is also possible for the even-surface odd-volumetric monopolar-RWG discretization of the EFIE, introduced in [6] with tetrahedral testing. This nonconforming discretization relies on the rearrangement of the monopolar-RWG space of current by two edge-oriented sets: the divergence-conforming RWG set and the nonconforming odd-monopolar-RWG set [6]. The testing of the fields is then carried out over pairs of adjacent triangles and wedges. Since the volumetric testing now is only required to capture half of the field contributions, the formulation appears more robust in terms of the choice of the heights of the volumetric testing elements with respect to the volumetric monopolar-RWG implementation, which requires full volumetric testing. This scheme, though, is mainly amenable to conformal triangulations because it requires the identification of the common edges between facets arising in the triangulation.

Manuscript received September 12, 2014; revised February 05, 2015; accepted April 18, 2015. This work was supported in part by the Spanish Interministerial Commission on Science and Technology (CICYT) and in part by the European Regional Development Fund (FEDER) under Projects TEC2010-20841-C04-02, TEC2012-37582-C04-02, and CONSOLIDER CSD2008-00068.

The authors are with the Department of Signal Theory and Communications, Universitat Politècnica de Catalunya, Barcelona 08034, Spain (e-mail: ubeda@tsc.upc.edu; rius@tsc.upc.edu; heldring@tsc.upc.edu; ivan.sekulic@tsc.upc.edu).

Q1

Color versions of one or more of the figures in this communication are available online at http://ieeexplore.ieee.org.

Digital Object Identifier 10.1109/TAP.2015.2426793

II. Wedges for Testing Purposes

A. Wedges Conformal to the Boundary

In conformal triangulations, the three trapezoids at the side faces of the qth wedge W_q are defined over the planes that bisect the angles formed by the qth surface triangle S_q and the adjacent triangles (see Fig. 1). The sides of the qth wedge connecting the vertices of top and bottom triangular faces are oriented along the directions given by the unit vectors $\boldsymbol{n}_q^{v,1}$, $\boldsymbol{n}_q^{v,2}$, and $\boldsymbol{n}_q^{v,3}$, which are defined in modulo three arithmetic as

$$\boldsymbol{n}_q^{v,i} = \frac{\boldsymbol{n}_q^{s,i+1} \times \boldsymbol{n}_q^{s,i-1}}{\left\| \boldsymbol{n}_q^{s,i+1} \times \boldsymbol{n}_q^{s,i-1} \right\|} \quad i = 1, 2, 3 \tag{1}$$

where $\boldsymbol{n}_q^{s,i}$ denotes the unit vector normal to S_i^q, the ith side trapezoid of W_q.

In objects with abrupt convex geometrical singularities, though, for facets with at least one vertex located on an abrupt sharp-edge but with no sides matching a sharp-edge (see Fig. 2), the definition in (1) leads to wedges breaking out of the boundary surface. Since in this case the null field is not enforced strictly inside the body, the definition in (1) for the normal unit vector defined at the controverted vertex P needs to be modified. Instead, we adopt the normalized projection on the plane Π_q^p of $\boldsymbol{n}_p^v$ at the vertex P, as defined in Fig. 2. The unit vectors assigned to the other two vertices need to be revisited too, so that the top and bottom triangles of the wedge remain parallel.

B. Wedges Nonconformal to the Boundary

For nonconformal triangulations, arising from the interconnection of triangles with nonmatching edges, we adopt right triangular prisms as testing elements (see Fig. 3). This is analogous to the nonconformal tetrahedral definition in [6], where the off-surface vertices of the testing tetrahedral elements are oriented perpendicularly with respect to the surface triangles. Now the three quadrilaterals at the three side faces of the wedges become rectangles that are oriented perpendicularly with respect to the surface triangles. Moreover, the base and opposite triangles are translated copies. Of course, this definition, nonconformal to the boundary surface, may also be applied to conformal triangulations, which actually simplifies considerably the implementation described in the previous section. On the other hand, this definition allows the testing wedges to cross the boundary surface.

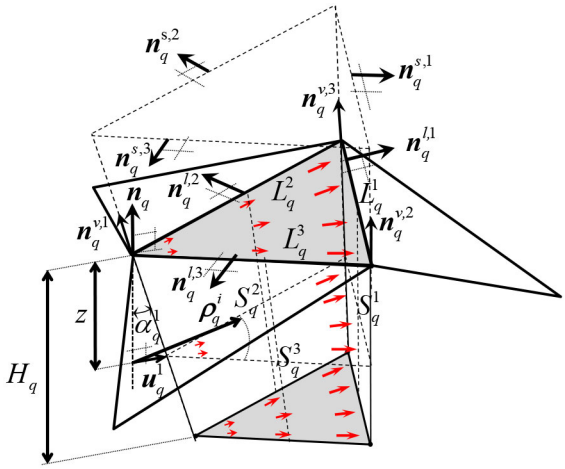

F1:1 Fig. 1. qth triangle of the surface triangulation that lies on top of the qth wedge
F1:2 of the volumetric distribution inside the object.

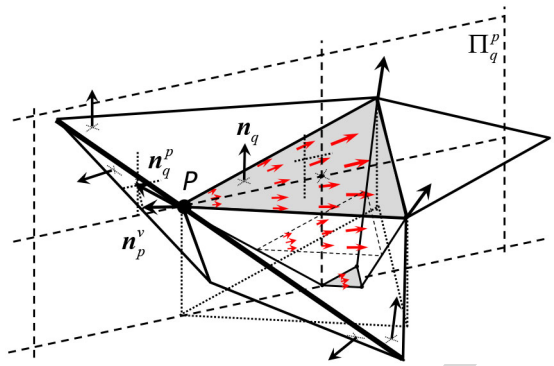

F2:1 Fig. 2. Confinement of the qth wedge inside the body when bordering on an
F2:2 abrupt sharp-edge. The unit vector $\boldsymbol{n}_p^v$ results from the normalized summation
F2:3 of the unit vectors that are normal to the facets meeting at P. The plane Π_q^p is
F2:4 normal to the qth triangle and contains the vertex P and the triangle centroid.

III. Nonconforming Discretization of the EFIE With Testing Over Wedges

In each triangle arising from the discretization, the monopolar-RWG expansion carries out a linearly growing approximating scheme from each vertex toward the opposed edge. Therefore, in general, for closed meshes, the resulting matrix equation handles a number of unknowns of three times the number of triangles. In conformal triangulations, this expansion gives rise to two independent unknowns at both sides of each edge.

A. Volumetric Discretization of the EFIE

We develop the volumetric monopolar-RWG discretization of the EFIE by the definition of three testing functions at each wedge. This is advantageous if compared with the tetrahedral testing described in [6], where the three testing functions associated with a particular surface triangle are defined over three different tetrahedral elements.

We define the "wedge-monopolar" testing function linked to the ith vertex of S_q in cylindrical coordinates, with the z-axis at this vertex oriented along $\boldsymbol{n}_q$, the unit vector perpendicular to S_q, as

$$\boldsymbol{P}_i^q(\rho,z) = \frac{1}{2A_qH_q}\left(\boldsymbol{\rho}_q^i - z\tan\alpha_q^i\boldsymbol{u}_q^i\right) \quad 1\le q\le N, 1\le i\le 3, 0\le z\le H_q \tag{2}$$

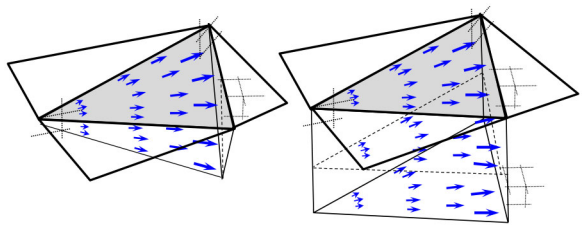

Fig. 3. Tetrahedral and wedge testing elements, nonconformal to the boundary surface. F3:1 F3:2

where N and A_q denote, respectively, the number of triangles and the area of S_q. The vector $\boldsymbol{\rho}_q^i$ represents the radial position vector of the observation point associated with the ith vertex. The variable z denotes the distance from S_q to the observation point. Note that the wedge-monopolar function in (2) is linearly growing and becomes zero along the edge of W_q meeting the ith vertex. In our numerical tests, we define the height H_q of W_q as a fraction of the mesh parameter h, which represents the average side length of the surface triangle. The parameter α_q^i denotes the angle between the directions given by $\boldsymbol{n}_q$ and $\boldsymbol{n}_q^{v,i}$(see Fig. 1). The unit vector $\boldsymbol{u}_q^i$ is parallel to S_q and is defined as

$$\boldsymbol{u}_q^i = \frac{\boldsymbol{n}_q - \boldsymbol{n}_q^{v,i}}{\left\|\boldsymbol{n}_q - \boldsymbol{n}_q^{v,i}\right\|}. \tag{3}$$

The nonconformal wedge definition, based on right triangular prisms, implies $\boldsymbol{n}_q^{v,i} = \boldsymbol{n}_q$ and $\alpha_q^i = 0$; hence, the definition in (2) is reduced to

$$\boldsymbol{P}_q^i(\rho,z) = \frac{1}{2A_qH_q}\boldsymbol{\rho}_q^i \quad 1\le q\le Nt,\ 1\le i\le 3. \tag{4}$$

The divergence of the testing functions is uniform over the qth facet in both scenarios and yields

$$\nabla\cdot\boldsymbol{P}_q^i = \frac{1}{A_qH_q} \quad i=1,2,3. \tag{5}$$

In this communication, we choose to define the monopolar-RWG basis functions in terms of facets, rather than edges as in [6]. This allows a general definition for the matrix system, valid for either conformal or nonconformal triangulations. The monopolar-RWG basis function associated with the pth vertex of the nth triangular facet is then defined as [1], [7]

$$\boldsymbol{g}_n^p(r) = \frac{1}{2A_n}\left(\boldsymbol{r}-\boldsymbol{r}_n^p\right) \quad p=1,2,3 \tag{6}$$

where the vector $\boldsymbol{r}_n^p$ denotes the position vector of the pth vertex of the source triangle S_n.

The resulting matrix system for the volumetric monopolar-RWG discretization of the EFIE, with testing over wedges, relies on [6] but adopts the wedge-monopolar definitions in (2) and (5). The resulting system then becomes

$$E_{\text{inc}}^{[q,i]} = \sum_{n=1}^{Nt}\sum_{p=1}^{3}\left[\mathrm{Z}_{[n,p]}^{A,[q,i]} + \mathrm{Z}_{[n,p]}^{\Phi,[q,i]}\right]c_{[n,p]} \quad 1\le q\le N,\ 1\le i\le 3 \tag{7}$$

where $c_{[n,p]}$ denotes the current coefficient of the monopolar-RWG function associated with the pth vertex of the nth triangle. The excitation vector yields

$$E_{\text{inc}}^{[q,i]} = \iiint_{W_q}\boldsymbol{P}_q^i(\boldsymbol{r})\cdot\boldsymbol{E}^{\text{inc}}dv \tag{8}$$

where $\boldsymbol{E}^{\mathrm{inc}}$ represents the electric-field vector impinging on the conductor. The vector-potential and scalar-potential contributions to the impedance elements $\mathrm{Z}^{A,[q,i]}_{[n,p]}$ and $\mathrm{Z}^{\Phi,[q,i]}_{[n,p]}$, respectively, become

$$\mathrm{Z}^{A,[q,i]}_{[n,p]} = jk\eta_0 \iiint\limits_{W_q} \boldsymbol{P}^i_q(\boldsymbol{r}) \cdot \iint\limits_{S_n} G(\boldsymbol{r},\boldsymbol{r}')\, \boldsymbol{g}^p_n(\boldsymbol{r}')\, ds' dv \tag{9}$$

$$\begin{aligned}\mathrm{Z}^{\Phi,[q,i]}_{[n,p]} = {} & j\frac{\eta_0}{k} \iint\limits_{S^q_i} \left(\boldsymbol{P}^i_q(\boldsymbol{r}) \cdot \boldsymbol{n}^{s,i}_q\right) \iint\limits_{S_n} G(\boldsymbol{r},\boldsymbol{r}')\, \nabla' \cdot \boldsymbol{g}^p_n(\boldsymbol{r}')\, ds' ds \\ & - j\frac{\eta_0}{k} \iiint\limits_{W_q} \nabla \cdot \boldsymbol{P}^i_q(\boldsymbol{r}) \iint\limits_{S_n} G(\boldsymbol{r},\boldsymbol{r}')\, \nabla' \cdot \boldsymbol{g}^p_n(\boldsymbol{r}')\, ds' dv \\ & - j\frac{\eta_0}{k} \iint\limits_{S^q_i} \left(\boldsymbol{P}^i_q(\boldsymbol{r}) \cdot \boldsymbol{n}^{s,i}_q\right) \int\limits_{L^n_p} G(\boldsymbol{r},\boldsymbol{r}') \left(\boldsymbol{g}^p_n(\boldsymbol{r}') \cdot \boldsymbol{n}^{l,p}_n\right) dl' ds \\ & + j\frac{\eta_0}{k} \iiint\limits_{W_q} \nabla \cdot \boldsymbol{P}^i_q(\boldsymbol{r}) \int\limits_{L^n_p} G(\boldsymbol{r},\boldsymbol{r}') \left(\boldsymbol{g}^p_n(\boldsymbol{r}') \cdot \boldsymbol{n}^{l,p}_n\right) dl' dv\end{aligned} \tag{10}$$

where G and L^n_p denote, respectively, the free-space Green's function and the segment opposed to the pth vertex in the nth source triangle (see Fig. 1). Note that for the testing nonconformal to the boundary surface, the implementation of (10) becomes somewhat easier (e.g., $\boldsymbol{n}^{s,i}_q = \boldsymbol{n}^{l,i}_q$).

B. Even-Surface Odd-Volumetric Discretization of the EFIE

The resulting matrix system for the even-surface odd-volumetric implementation and wedge testing derives from [6] through (19)–(30), with the wedge-monopolar definitions in (2), (4), and (5). The testing wedges can also be conformal or nonconformal to the boundary surface. For electrically moderate or big sharp-edged objects, handling a considerable amount of unknowns, we implement the hybrid even-surface odd-volumetric monopolar-RWG discretization of the EFIE, which reduces the computational cost while preserving the accuracy. Indeed, the odd monopolar-RWG basis functions are only defined at those edges in the meshing matching the sharp edges of the object [6].

IV. Numerical Results

We illustrate for several sharp-edged objects the observed improved accuracy with respect to the RWG-discretization of the EFIE, EFIE[RWG], of the monopolar-RWG discretizations of the EFIE; namely, volumetric, EFIE[monoRWG], and even-surface odd-volumetric, EFIE[e-o-monoRWG]. In Sections IV-A and IV-B, we plot RCS and near-field errors for closed conformal triangulations against the height of the testing elements H and the number of unknowns, respectively. The reference RCS results are computed with the RWG-discretization of the EFIE and extremely fine meshes (of about 70 000 unknowns) [6]. In Section IV-C, we plot RCS results for a composite object meshed with a nonconformal triangulation. We compute the inner surface and volumetric integrals in the impedance elements through the singularity subtraction of the $R^{-1}-\mathrm{Kernel}$ contributions [8]. The outer integrals and the remaining low-order Kernel contributions in the inner integrals are evaluated numerically with Gaussian rules [6], [9], [10]. The volumetric integrals over wedges are computed through the decomposition of each wedge into three tetrahedral elements. An x-polarized z-propagating plane wave is impinging on the tested conductors.

A. Accuracy Versus H

In Figs. 4, 5(a), and 6(a), relative RCS-errors are shown for volumetric monopolar-RWG discretizations of the EFIE in terms of the height

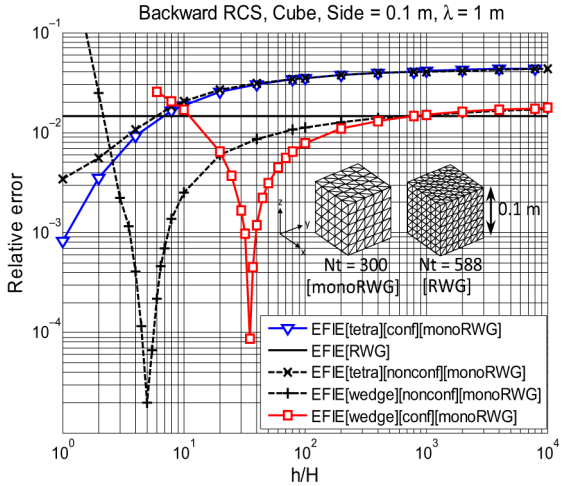

Fig. 4. Relative error of the backward scattered RCS versus the height H, defined as a fraction of the mesh parameter h, of the testing elements with several EFIE-implementations for a cube with side 0.1 m ($\lambda = 1$ m). The meshes employ 300 and 588 triangles for the monopolar-RWG and RWG discretizations.

of the testing elements for a degree of meshing with respect to the relative error of EFIE[RWG] and finer triangulation but similar number of unknowns. The tested objects are, respectively, a cube with side 0.1λ, a regular pyramid with square basis and side 0.1λ and a regular tetrahedron with side 0.1λ ($\lambda = 1$ m). In light of these figures, the volumetric monopolar-RWG discretization of the EFIE with testing over wedges shows improved accuracy with respect to EFIE[RWG] for a wider range of values of H than with tetrahedral testing. The ranges of H with observed improved accuracy for testing over wedges lie between $h/10$ and $h/10^3$, for the moderately small sharp-edged objects, and between $h/10^2$ and $h/10^4$ for the 1λ-tetrahedron. These H ranges include both wedge choices, conformal, [conf], or nonconformal [nonconf], to the boundary surface, and are one order of magnitude bigger than the H ranges with observed improved accuracy for the tetrahedral testing, which lie roughly between h and $h/10$.

The volumetric monopolar-RWG discretization of the EFIE with testing wedges conformal to the boundary surface shows improved accuracy for a wider range of H with respect to the nonconformal choice for the square-pyramid, which is an example of electrically small sharp-edged object with abrupt sharp-edge. In any case, for small enough values of H, around $h/100$ or smaller, the performance of both wedge testing choices, conformal or nonconformal to the boundary surface, becomes increasingly similar, showing improved or similar performance with respect to EFIE[RWG] for all the tested objects. With tetrahedral testing, the conformal and nonconformal choices become also similar for small values of H (below $h/10$) but with evident loss of accuracy.

In Figs. 5(b) and 6(b), we show RCS results for the even-surface odd-volumetric monopolar-RWG discretizations of the EFIE. In Fig. 5(b), for the 0.1λ-square pyramid, this is the complete implementation, handling twice the number of edges as number of unknowns. In Fig. 6(b), for the 1λ-tetrahedron, an object with moderate electrical dimensions, the even-surface odd-volumetric implementation is hybrid, whereby the number of unknowns is reduced to the edges arising in the triangulation plus the edges matching the sharp edges of the object [6]. In view of these figures, the wedge testing shows improved RCS-accuracy in similar terms as the corresponding implementations with tetrahedral testing [6]. Similarly, the observed performance now with the even-surface odd-volumetric implementations is less dependent on the testing choices, conformal or nonconformal to the

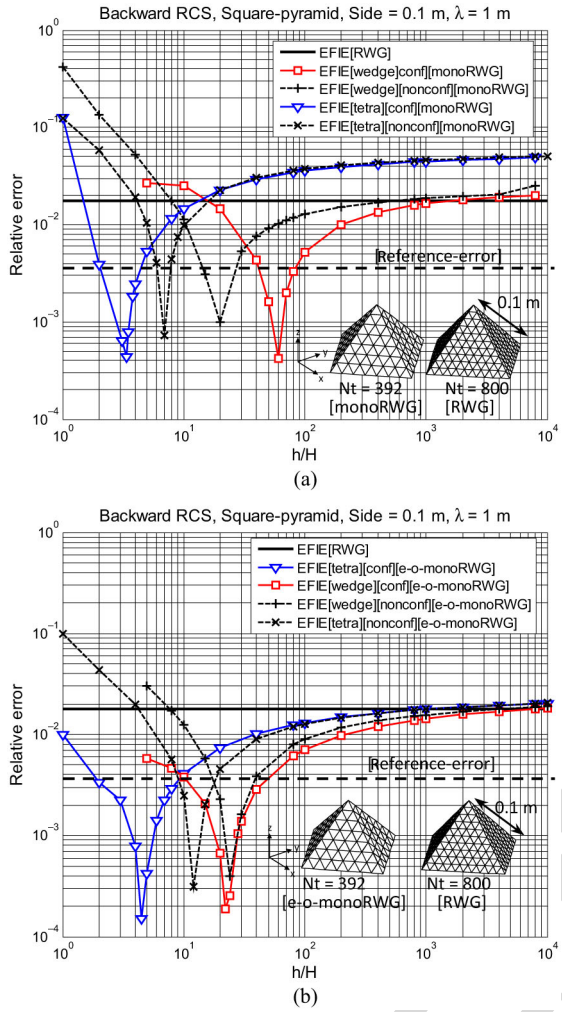

F5:1 Fig. 5. Relative error for a pyramid with square basis with side 0.1λ ($\lambda = 1$ m)
F5:2 of the backward scattered RCS versus the height H, defined as a fraction of the
F5:3 mesh parameter h, of the testing elements computed with several monopolar-
F5:4 RWG EFIE-implementations. (a) Volumetric. (b) Even-surface odd-volumetric.
F5:5 The meshes make use of 392 triangles for the monopolar-RWG and even-
F5:6 odd-monopolar-RWG discretizations; for the RWG-discretization, the mesh
F5:7 employs 800 triangles.

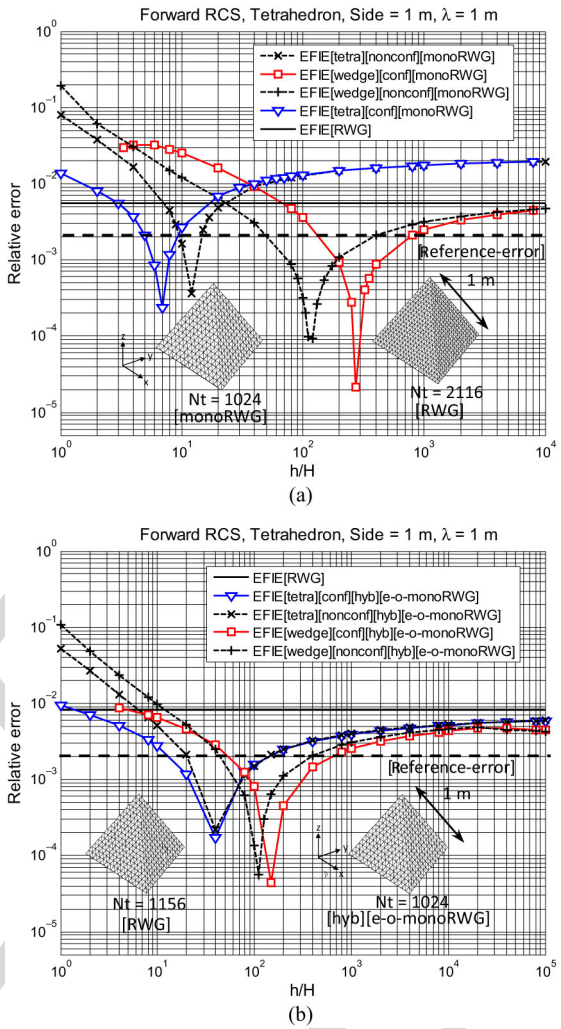

F6:1 Fig. 6. Relative error for a tetrahedron with side 1λ ($\lambda = 1$ m) of the for-
F6:2 ward scattered RCS versus the height H, defined as a fraction of the mesh
F6:3 parameter h, of the testing elements with several monopolar-RWG implemen-
F6:4 tations of the EFIE. (a) Volumetric. (b) Hybrid even-surface odd-volumetric.
F6:5 The meshes adopt 1024 triangles for the monopolar-RWG and hybrid even-
F6:6 odd-monopolarRWG discretizations; for the RWG-discretization, the meshes
F6:7 employ 2116 triangles in (a) and 1156 triangles in (b).

boundary surface, than their volumetric counterparts. Furthermore, the H range with improved accuracy for the even-surface odd-volumetric discretization with wedge testing is notoriously bigger than the ranges observed for the volumetric discretization and same testing choice. In particular, the H range with improved accuracy for EFIE[e-o-monoRWG] and the square pyramid lies between h and $h/10^4$, whereas for EFIE[hyb][e-o-monoRWG] and the tetrahedron, between h and $h/10^5$. This involves at least two orders of magnitude bigger than the observed H ranges for EFIE[wedge][monoRWG].

In Fig. 7, we plot, for the 0.1λ square pyramid, the near-field relative error in terms of H and fixed degree of meshing for the monopolar-RWG discretizations of the EFIE at a point inside the object, at a distance of 0.02 m of the top vertex along the pyramid axis. We define the near-field error as the ratio between the magnitudes of the total and incident electric fields at that point [6]. As discussed in detail in [6], the observed improved far-field accuracy prevails in the near-field especially for electrically small objects. Indeed, in view of Fig. 7, the best-performing H-values for each discretization are consistent with the observed trends in Fig. 5 for the computed far-field.

B. Accuracy Versus N

In Figs. 8 and 9, we show for the square pyramid and the tetrahedron, respectively, the relative error of the RCS computed with the nonconforming EFIE-implementations with respect to reliable RCS references against the number of unknowns. For each implementation and object, we show two graphs corresponding to two H values that are 10 and 100 times smaller than certain H values leading to the same reference errors (see Figs. 5 and 6). For the square pyramid, this error is 3.5e-3, whereas for the tetrahedron, it is 2e-3. In view of Figs. 5 and 6, for the volumetric implementations, the corresponding reference H-values are: 1) for the square pyramid, $h/42$ (wedge) and $h/2$ (tetrahedral) and 2) for the tetrahedron, $h/120$ (wedge) and $h/5$ (tetrahedral). Similarly, these H values for the even-surface odd-volumetric implementations become: 1) for the square pyramid, $h/10$ (wedge) and $h/2$ (tetrahedral) and 2) for the tetrahedron, $h/50$ (wedge) and $h/13$ (tetrahedral).

The computed RCS over these ranges with the volumetric monopolar-RWG discretization of the EFIE and wedge testing

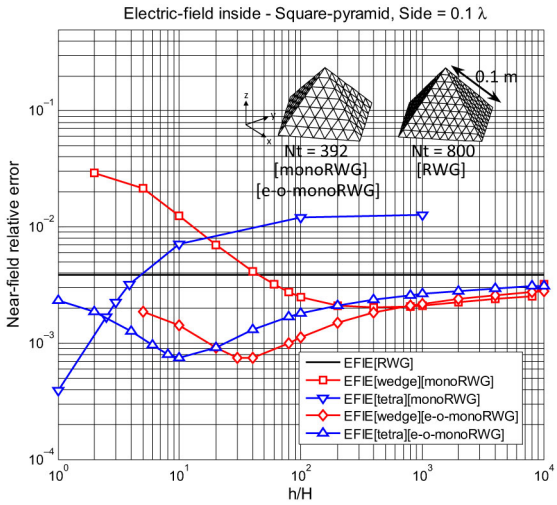

F7:1 Fig. 7. Near-field relative error inside the object versus the height H of the
F7:2 testing elements, with several monopolar-RWG EFIE-implementations for a
F7:3 square pyramid with side 0.1 m ($\lambda = 1$ m). The testing point is at distance
F7:4 of 0.02 m of the top vertex along the pyramid axis. The testing elements are
F7:5 defined conformal to the boundary surface.

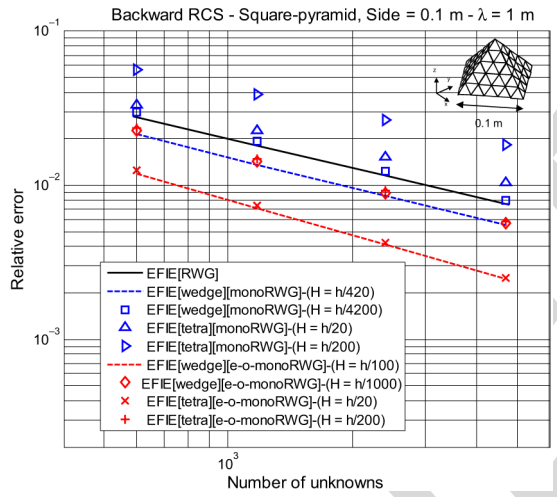

F8:1 Fig. 8. Relative error of the backward scattered RCS versus the number of
F8:2 unknowns computed with several monopolar-RWG EFIE-implementations for
F8:3 a square pyramid with side $= 0.1$ m ($\lambda = 1$ m). The testing elements are
F8:4 defined conformal to the boundary surface.

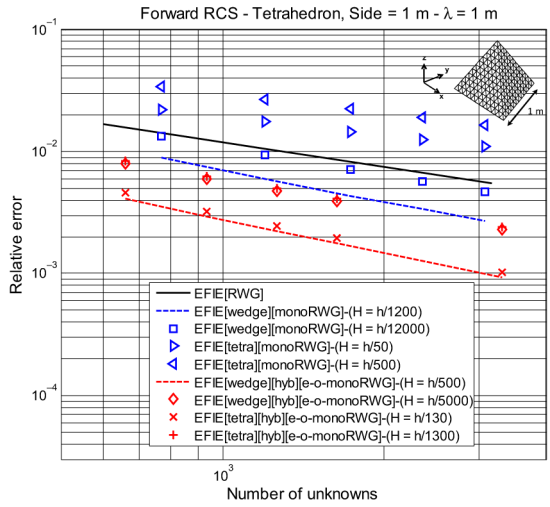

Fig. 9. Relative error of the forward scattered RCS versus the number of unknowns computed with several monopolar-RWG EFIE-implementations for a regular tetrahedron with side $= 1$ m ($\lambda = 1$ m). The testing elements are defined conformal to the boundary surface. F9:1 F9:2 F9:3 F9:4

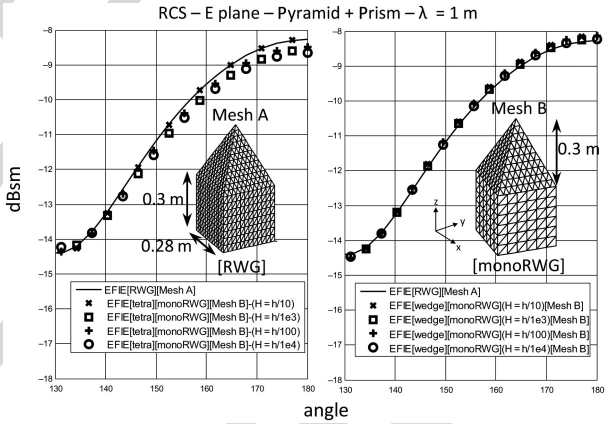

Fig. 10. xz plane cut of the RCS computed with several EFIE-implementations for an object composed of a pyramid on top of a rectangular prism. Meshes A and B employ, respectively, 1920 and 832 triangles. F10:1 F10:2 F10:3

produces smaller error than the tetrahedral choice and the RWG-discretization (see Figs. 8 and 9). In contrast, the wedge and tetrahedral testing choices for the even-surface odd-volumetric monopolar-RWG discretization produce very similar performance, which is a sign of robustness. Moreover, the observed errors with the even-surface odd-volumetric implementations in both objects become much smaller than for the volumetric implementations.

C. Nonconformal Triangulations

In Fig. 10, we show the RCS for the composite object arising from the juxtaposition of a pyramid with rectangular basis on top of a rectangular prism. Two meshes are used: 1) a closed conformal mesh of 1920 triangles (mesh A) and 2) a nonconformal mesh of 832 triangles resulting from the interconnection of two independent open triangulations (mesh B). Neither the RWG-discretization nor the even-surface odd-volumetric monopolar-RWG discretization of the EFIE can handle the mesh B, where some neighboring triangles have nonmatching edges. Instead, the volumetric monopolar-RWG discretization, with the testing elements defined nonconformal to the boundary surface, stands for a flexible and versatile tool, well suited for the analysis of Mesh B. It is clear from Fig. 10 that the wedge testing in the volumetric monopolar-RWG discretization of the EFIE results in a more stable performance in terms of H than the tetrahedral testing.

V. Conclusion

The adoption of testing wedges conformal to the boundary surface in the volumetric monopolar-RWG discretization of the EFIE shows, for the sharp-edged conductors tested, improved accuracy for a wider range of heights of the testing elements than the choice of tetrahedral elements (between $h/10$ and $h/10^3$, for the moderately small objects tested, and between $h/10^2$ and $h/10^4$ for the 1λ-tetrahedron). For small enough heights, below one-hundredth of the mesh parameter, right triangular prisms, easy-to-implement, can be adopted too as successful testing elements. The even-surface odd-volumetric

monopolar-RWG discretization of the EFIE with wedge testing performs in a similar manner as described in [6] for tetrahedral testing elements. These implementations reach, for the sharp-edged conductors tested, much wider ranges of heights of the testing elements with improved accuracy (at least two orders of magnitude bigger than for the volumetric monopolar-RWG discretization and wedge testing).

For composite objects meshed with nonconformal triangulations where neighboring triangles have no matching edges, the volumetric monopolar-RWG discretization of the EFIE with testing over right triangular prisms appears as a more reliable option than the choice with tetrahedral testing because the computed RCS becomes more stable in terms of the heights of the testing elements. The even-surface odd-volumetric monopolar-RWG implementation, though, which assigns unknowns to the edges between pairs of adjacent facets, is not amenable in general to such triangulations.

We believe that the better suitability of the wedges as testing elements when compared with the tetrahedral elements lies in the fact that the wedge-monopolar testing functions enforce the null condition for the component of the inner electric field tangential to the boundary surface, which shows better consistency with the electric-field boundary condition at the surface.

REFERENCES

[1] S. M. Rao, D. R. Wilton, and A. W. Glisson, "Electromagnetic scattering by surfaces of arbitrary shape," *IEEE Trans. Antennas Propag.*, vol. 30, no. 3, pp. 409–418, May 1982.

[2] R. D. Graglia, D. R. Wilton, and A. F. Peterson, "Higher order interpolatory vector bases for computational electromagnetics," *IEEE Trans. Antennas Propag.*, vol. 45, no. 3, pp. 329–342, Mar. 1997.

[3] M. Carr, E. Topsakal, and J. L. Volakis, "A procedure for modeling material junctions in 3-D surface integral equation approaches," *IEEE Trans. Antennas Propag.*, vol. 52, no. 5, pp. 1374–1379, May 2004.

[4] P. Ylä-Oijala, M. Taskinen, and J. Sarvas, "Surface integral equation method for general composite metallic and dielectric structures with junctions," *Prog. Electromagn. Res.*, vol. 52, pp. 81–108, 2005.

[5] E. Ubeda, J. M. Rius, and A. Heldring, "Discretization of the EFIE in method of moments without continuity of the normal current component across edges," in *Proc. IEEE Antennas Propag. Soc. Int. Symp.*, Orlando, FL, USA, Jul. 7–13, 2013, pp. 448–449.

[6] E. Ubeda, J. M. Rius, and A. Heldring, "Nonconforming discretization of the electric-field integral equation for closed perfectly conducting objects," *IEEE Trans. Antennas Propag.*, vol. 62, no. 8, pp. 4171–4186, Aug. 2014.

[7] E. Ubeda and J. M. Rius, "Monopolar divergence-conforming and curl-conforming low-order basis functions for the electromagnetic scattering analysis," *Microw. Opt. Technol. Lett.*, vol. 46, no. 3, pp. 237–241, Aug. 2005.

[8] D. R. Wilton *et al.*, "Potential integrals for uniform and linear source distributions on polygonal and polyhedral domains," *IEEE Trans. Antennas Propag.*, vol. 32, no. 3, pp. 276–281, Mar. 1984.

[9] D. A. Dunavant, "High degree efficient symmetrical Gaussian quadrature rules for the triangle," *Int. J. Numer. Methods Eng.*, vol. 21, pp. 1129–1148, 1985.

[10] M. Gellert and R. Harbord, "Moderate degree cubature formulas for 3-D tetrahedral finite element approximations," *Commun. Appl. Numer. Methods*, vol. 7. pp. 487–495, 1991.

QUERY

Q1: Please check and confirm the inserted affiliation.

Volumetric Testing Parallel to the Boundary Surface for a Nonconforming Discretization of the Electric-Field Integral Equation

Eduard Ubeda, Juan M. Rius, Alex Heldring, and Ivan Sekulic

***Abstract*—The volumetric monopolar-RWG discretization of the electric-field integral equation (EFIE) imposes no continuity constraint across edges in the surface discretization around a closed conductor. The current is expanded with the monopolar-RWG set and the electric field is tested over a set of tetrahedral elements attached to the boundary surface. This scheme is facet-oriented and therefore, well suited for the scattering analysis of nonconformal meshes or composite objects. The observed accuracy, though, is only competitive with respect to the RWG-discretization for a restricted range of heights of the tetrahedral elements. In this communication, we introduce a novel implementation of the volumetric monopolar-RWG discretization of the EFIE with testing over a set of wedges. We show with RCS and near-field results that this scheme offers improved accuracy for a wider range of heights than the approach with tetrahedral testing. The application of the wedge testing to the even-surface odd-volumetric monopolar-RWG discretization of the EFIE, edge-oriented and therefore less versatile, shows similar accuracy as with tetrahedral testing, which is a sign of robustness.**

***Index Terms*—Basis functions, electric-field integral equation (EFIE), integral equations, moment method.**

I. Introduction

The discretization of the electric-field integral equation (EFIE) for perfectly conducting objects is very often based on the low-order divergence-conforming RWG basis functions [1], [2]. The application of the edge-oriented RWG basis functions to composite objects, with piecewise homogeneous regions, brings out some pitfalls: 1) if the adopted mesh is conformal, the imposition of normal current continuity around junctions becomes very awkward [3], [4] and 2) if the adopted mesh is nonconformal, arising from the interconnection of triangulations with nonmatching edges, the RWG basis functions cannot be used. In these scenarios, a facet-oriented implementation of the EFIE, like the recently proposed volumetric monopolar-RWG discretization of the EFIE [5], [6], appears better suited: 1) the current is expanded with the monopolar-RWG basis functions, with no continuity across edges [7] and 2) the fields are tested over a set of tetrahedral elements attached to the surface triangulation, inside the body, to make the hyper-singular Kernel contributions numerically manageable.

In this communication, we present a new implementation of the volumetric monopolar-RWG discretization of the EFIE, so that the field testing is carried out over a set of wedges attached to the surface triangulation. Although this approach adds some complexity in the definition of the testing elements, improved accuracy is observed when compared with the tetrahedral testing for a wider range of heights of the testing elements. The testing over wedges is also possible for the even-surface odd-volumetric monopolar-RWG discretization of the EFIE, introduced in [6] with tetrahedral testing. This nonconforming discretization relies on the rearrangement of the monopolar-RWG space of current by two edge-oriented sets: the divergence-conforming RWG set and the nonconforming odd-monopolar-RWG set [6]. The testing of the fields is then carried out over pairs of adjacent triangles and wedges. Since the volumetric testing now is only required to capture half of the field contributions, the formulation appears more robust in terms of the choice of the heights of the volumetric testing elements with respect to the volumetric monopolar-RWG implementation, which requires full volumetric testing. This scheme, though, is mainly amenable to conformal triangulations because it requires the identification of the common edges between facets arising in the triangulation.

Manuscript received September 12, 2014; revised February 05, 2015; accepted April 18, 2015. This work was supported in part by the Spanish Interministerial Commission on Science and Technology (CICYT) and in part by the European Regional Development Fund (FEDER) under Projects TEC2010-20841-C04-02, TEC2012-37582-C04-02, and CONSOLIDER CSD2008-00068.

The authors are with the Department of Signal Theory and Communications, Universitat Politècnica de Catalunya, Barcelona 08034, Spain (e-mail: ubeda@tsc.upc.edu; rius@tsc.upc.edu; heldring@tsc.upc.edu; ivan.sekulic@tsc.upc.edu).

Color versions of one or more of the figures in this communication are available online at http://ieeexplore.ieee.org.

Digital Object Identifier 10.1109/TAP.2015.2426793

II. Wedges for Testing Purposes

A. Wedges Conformal to the Boundary

In conformal triangulations, the three trapezoids at the side faces of the qth wedge W_q are defined over the planes that bisect the angles formed by the qth surface triangle S_q and the adjacent triangles (see Fig. 1). The sides of the qth wedge connecting the vertices of top and bottom triangular faces are oriented along the directions given by the unit vectors $\boldsymbol{n}_q^{v,1}$, $\boldsymbol{n}_q^{v,2}$, and $\boldsymbol{n}_q^{v,3}$, which are defined in modulo three arithmetic as

$$\boldsymbol{n}_q^{v,i} = \frac{\boldsymbol{n}_q^{s,i+1} \times \boldsymbol{n}_q^{s,i-1}}{\left\| \boldsymbol{n}_q^{s,i+1} \times \boldsymbol{n}_q^{s,i-1} \right\|} \quad i = 1, 2, 3 \tag{1}$$

where $\boldsymbol{n}_q^{s,i}$ denotes the unit vector normal to S_i^q, the ith side trapezoid of W_q.

In objects with abrupt convex geometrical singularities, though, for facets with at least one vertex located on an abrupt sharp-edge but with no sides matching a sharp-edge (see Fig. 2), the definition in (1) leads to wedges breaking out of the boundary surface. Since in this case the null field is not enforced strictly inside the body, the definition in (1) for the normal unit vector defined at the controverted vertex P needs to be modified. Instead, we adopt the normalized projection on the plane Π_q^p of $\boldsymbol{n}_p^v$ at the vertex P, as defined in Fig. 2. The unit vectors assigned to the other two vertices need to be revisited too, so that the top and bottom triangles of the wedge remain parallel.

B. Wedges Nonconformal to the Boundary

For nonconformal triangulations, arising from the interconnection of triangles with nonmatching edges, we adopt right triangular prisms as testing elements (see Fig. 3). This is analogous to the nonconformal tetrahedral definition in [6], where the off-surface vertices of the testing tetrahedral elements are oriented perpendicularly with respect to the surface triangles. Now the three quadrilaterals at the three side faces of the wedges become rectangles that are oriented perpendicularly with respect to the surface triangles. Moreover, the base and opposite triangles are translated copies. Of course, this definition, nonconformal to the boundary surface, may also be applied to conformal triangulations, which actually simplifies considerably the implementation described in the previous section. On the other hand, this definition allows the testing wedges to cross the boundary surface.

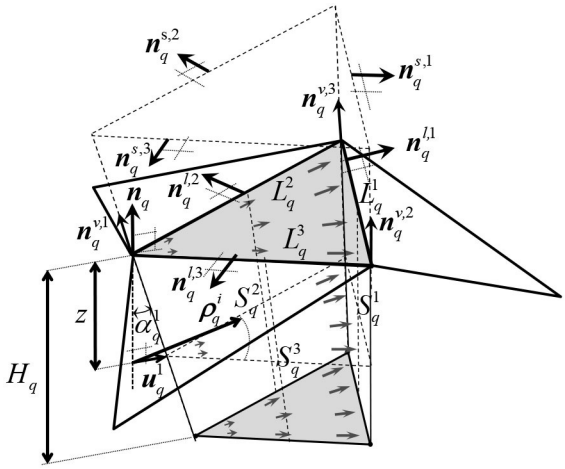

F1:1 Fig. 1. qth triangle of the surface triangulation that lies on top of the qth wedge
F1:2 of the volumetric distribution inside the object.

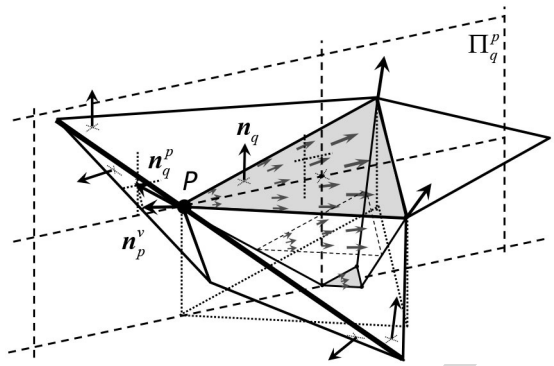

F2:1 Fig. 2. Confinement of the qth wedge inside the body when bordering on an
F2:2 abrupt sharp-edge. The unit vector $\boldsymbol{n}_p^v$ results from the normalized summation
F2:3 of the unit vectors that are normal to the facets meeting at P. The plane Π_q^p is
F2:4 normal to the qth triangle and contains the vertex P and the triangle centroid.

III. Nonconforming Discretization of the EFIE With Testing Over Wedges

In each triangle arising from the discretization, the monopolar-RWG expansion carries out a linearly growing approximating scheme from each vertex toward the opposed edge. Therefore, in general, for closed meshes, the resulting matrix equation handles a number of unknowns of three times the number of triangles. In conformal triangulations, this expansion gives rise to two independent unknowns at both sides of each edge.

A. Volumetric Discretization of the EFIE

We develop the volumetric monopolar-RWG discretization of the EFIE by the definition of three testing functions at each wedge. This is advantageous if compared with the tetrahedral testing described in [6], where the three testing functions associated with a particular surface triangle are defined over three different tetrahedral elements.

We define the "wedge-monopolar" testing function linked to the ith vertex of S_q in cylindrical coordinates, with the z-axis at this vertex oriented along $\boldsymbol{n}_q$, the unit vector perpendicular to S_q, as

$$\boldsymbol{P}_i^q(\rho,z) = \frac{1}{2A_qH_q}\left(\boldsymbol{\rho}_q^i - z\tan\alpha_q^i\boldsymbol{u}_q^i\right) \quad 1\le q\le N, 1\le i\le 3, 0\le z\le H_q \tag{2}$$

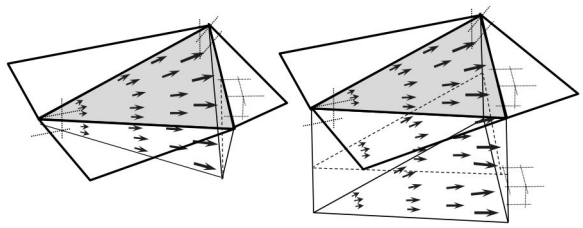

Fig. 3. Tetrahedral and wedge testing elements, nonconformal to the boundary surface. F3:1 F3:2

where N and A_q denote, respectively, the number of triangles and the area of S_q. The vector $\boldsymbol{\rho}_q^i$ represents the radial position vector of the observation point associated with the ith vertex. The variable z denotes the distance from S_q to the observation point. Note that the wedge-monopolar function in (2) is linearly growing and becomes zero along the edge of W_q meeting the ith vertex. In our numerical tests, we define the height H_q of W_q as a fraction of the mesh parameter h, which represents the average side length of the surface triangle. The parameter α_q^i denotes the angle between the directions given by $\boldsymbol{n}_q$ and $\boldsymbol{n}_q^{v,i}$(see Fig. 1). The unit vector $\boldsymbol{u}_q^i$ is parallel to S_q and is defined as

$$\boldsymbol{u}_q^i = \frac{\boldsymbol{n}_q - \boldsymbol{n}_q^{v,i}}{\left\|\boldsymbol{n}_q - \boldsymbol{n}_q^{v,i}\right\|}. \tag{3}$$

The nonconformal wedge definition, based on right triangular prisms, implies $\boldsymbol{n}_q^{v,i} = \boldsymbol{n}_q$ and $\alpha_q^i = 0$; hence, the definition in (2) is reduced to

$$\boldsymbol{P}_q^i(\rho,z) = \frac{1}{2A_qH_q}\boldsymbol{\rho}_q^i \quad 1\le q\le Nt,\ 1\le i\le 3. \tag{4}$$

The divergence of the testing functions is uniform over the qth facet in both scenarios and yields

$$\nabla\cdot\boldsymbol{P}_q^i = \frac{1}{A_qH_q} \quad i=1,2,3. \tag{5}$$

In this communication, we choose to define the monopolar-RWG basis functions in terms of facets, rather than edges as in [6]. This allows a general definition for the matrix system, valid for either conformal or nonconformal triangulations. The monopolar-RWG basis function associated with the pth vertex of the nth triangular facet is then defined as [1], [7]

$$\boldsymbol{g}_n^p(r) = \frac{1}{2A_n}\left(\boldsymbol{r}-\boldsymbol{r}_n^p\right) \quad p=1,2,3 \tag{6}$$

where the vector $\boldsymbol{r}_n^p$ denotes the position vector of the pth vertex of the source triangle S_n.

The resulting matrix system for the volumetric monopolar-RWG discretization of the EFIE, with testing over wedges, relies on [6] but adopts the wedge-monopolar definitions in (2) and (5). The resulting system then becomes

$$E_{\text{inc}}^{[q,i]} = \sum_{\text{n}=1}^{N_t}\sum_{p=1}^{3}\left[\text{Z}_{[n,p]}^{A,[q,i]} + \text{Z}_{[n,p]}^{\Phi,[q,i]}\right]c_{[n,p]} \quad 1\le q\le N,\ 1\le i\le 3 \tag{7}$$

where $c_{[n,p]}$ denotes the current coefficient of the monopolar-RWG function associated with the pth vertex of the nth triangle. The excitation vector yields

$$E_{\text{inc}}^{[q,i]} = \iiint_{W_q}\boldsymbol{P}_q^i(\boldsymbol{r})\cdot\boldsymbol{E}^{\text{inc}}dv \tag{8}$$

where $\boldsymbol{E}^{\mathrm{inc}}$ represents the electric-field vector impinging on the conductor. The vector-potential and scalar-potential contributions to the impedance elements $\mathrm{Z}^{A,[q,i]}_{[n,p]}$ and $\mathrm{Z}^{\Phi,[q,i]}_{[n,p]}$, respectively, become

$$\mathrm{Z}^{A,[q,i]}_{[n,p]} = jk\eta_0 \iiint\limits_{W_q} \boldsymbol{P}^i_q(\boldsymbol{r}) \cdot \iint\limits_{S_n} G(\boldsymbol{r},\boldsymbol{r}')\, \boldsymbol{g}^p_n(\boldsymbol{r}')\, ds' dv \tag{9}$$

$$\begin{aligned}\mathrm{Z}^{\Phi,[q,i]}_{[n,p]} = {} & j\frac{\eta_0}{k} \iint\limits_{S^q_i} \left(\boldsymbol{P}^i_q(\boldsymbol{r}) \cdot \boldsymbol{n}^{s,i}_q\right) \iint\limits_{S_n} G(\boldsymbol{r},\boldsymbol{r}')\, \nabla' \cdot \boldsymbol{g}^p_n(\boldsymbol{r}')\, ds' ds \\ & - j\frac{\eta_0}{k} \iiint\limits_{W_q} \nabla \cdot \boldsymbol{P}^i_q(\boldsymbol{r}) \iint\limits_{S_n} G(\boldsymbol{r},\boldsymbol{r}')\, \nabla' \cdot \boldsymbol{g}^p_n(\boldsymbol{r}')\, ds' dv \\ & - j\frac{\eta_0}{k} \iint\limits_{S^q_i} \left(\boldsymbol{P}^i_q(\boldsymbol{r}) \cdot \boldsymbol{n}^{s,i}_q\right) \int\limits_{L^n_p} G(\boldsymbol{r},\boldsymbol{r}') \left(\boldsymbol{g}^p_n(\boldsymbol{r}') \cdot \boldsymbol{n}^{l,p}_n\right) dl' ds \\ & + j\frac{\eta_0}{k} \iiint\limits_{W_q} \nabla \cdot \boldsymbol{P}^i_q(\boldsymbol{r}) \int\limits_{L^n_p} G(\boldsymbol{r},\boldsymbol{r}') \left(\boldsymbol{g}^p_n(\boldsymbol{r}') \cdot \boldsymbol{n}^{l,p}_n\right) dl' dv \end{aligned} \tag{10}$$

where G and L^n_p denote, respectively, the free-space Green's function and the segment opposed to the pth vertex in the nth source triangle (see Fig. 1). Note that for the testing nonconformal to the boundary surface, the implementation of (10) becomes somewhat easier (e.g., $\boldsymbol{n}^{s,i}_q = \boldsymbol{n}^{l,i}_q$).

B. Even-Surface Odd-Volumetric Discretization of the EFIE

The resulting matrix system for the even-surface odd-volumetric implementation and wedge testing derives from [6] through (19)–(30), with the wedge-monopolar definitions in (2), (4), and (5). The testing wedges can also be conformal or nonconformal to the boundary surface. For electrically moderate or big sharp-edged objects, handling a considerable amount of unknowns, we implement the hybrid even-surface odd-volumetric monopolar-RWG discretization of the EFIE, which reduces the computational cost while preserving the accuracy. Indeed, the odd monopolar-RWG basis functions are only defined at those edges in the meshing matching the sharp edges of the object [6].

IV. Numerical Results

We illustrate for several sharp-edged objects the observed improved accuracy with respect to the RWG-discretization of the EFIE, EFIE[RWG], of the monopolar-RWG discretizations of the EFIE; namely, volumetric, EFIE[monoRWG], and even-surface odd-volumetric, EFIE[e-o-monoRWG]. In Sections IV-A and IV-B, we plot RCS and near-field errors for closed conformal triangulations against the height of the testing elements H and the number of unknowns, respectively. The reference RCS results are computed with the RWG-discretization of the EFIE and extremely fine meshes (of about 70 000 unknowns) [6]. In Section IV-C, we plot RCS results for a composite object meshed with a nonconformal triangulation. We compute the inner surface and volumetric integrals in the impedance elements through the singularity subtraction of the $R^{-1}-\mathrm{Kernel}$ contributions [8]. The outer integrals and the remaining low-order Kernel contributions in the inner integrals are evaluated numerically with Gaussian rules [6], [9], [10]. The volumetric integrals over wedges are computed through the decomposition of each wedge into three tetrahedral elements. An x-polarized z-propagating plane wave is impinging on the tested conductors.

A. Accuracy Versus H

In Figs. 4, 5(a), and 6(a), relative RCS-errors are shown for volumetric monopolar-RWG discretizations of the EFIE in terms of the height

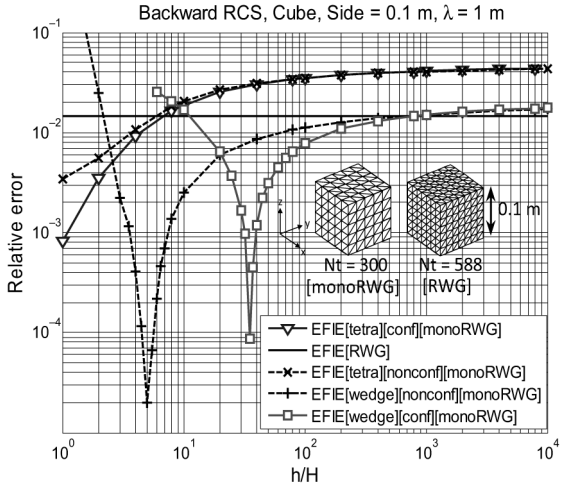

Fig. 4. Relative error of the backward scattered RCS versus the height H, defined as a fraction of the mesh parameter h, of the testing elements with several EFIE-implementations for a cube with side 0.1 m ($\lambda = 1$ m). The meshes employ 300 and 588 triangles for the monopolar-RWG and RWG discretizations.

of the testing elements for a degree of meshing with respect to the relative error of EFIE[RWG] and finer triangulation but similar number of unknowns. The tested objects are, respectively, a cube with side 0.1λ, a regular pyramid with square basis and side 0.1λ and a regular tetrahedron with side 0.1λ ($\lambda = 1$ m). In light of these figures, the volumetric monopolar-RWG discretization of the EFIE with testing over wedges shows improved accuracy with respect to EFIE[RWG] for a wider range of values of H than with tetrahedral testing. The ranges of H with observed improved accuracy for testing over wedges lie between $h/10$ and $h/10^3$, for the moderately small sharp-edged objects, and between $h/10^2$ and $h/10^4$ for the 1λ-tetrahedron. These H ranges include both wedge choices, conformal, [conf], or nonconformal [nonconf], to the boundary surface, and are one order of magnitude bigger than the H ranges with observed improved accuracy for the tetrahedral testing, which lie roughly between h and $h/10$.

The volumetric monopolar-RWG discretization of the EFIE with testing wedges conformal to the boundary surface shows improved accuracy for a wider range of H with respect to the nonconformal choice for the square-pyramid, which is an example of electrically small sharp-edged object with abrupt sharp-edge. In any case, for small enough values of H, around $h/100$ or smaller, the performance of both wedge testing choices, conformal or nonconformal to the boundary surface, becomes increasingly similar, showing improved or similar performance with respect to EFIE[RWG] for all the tested objects. With tetrahedral testing, the conformal and nonconformal choices become also similar for small values of H (below $h/10$) but with evident loss of accuracy.

In Figs. 5(b) and 6(b), we show RCS results for the even-surface odd-volumetric monopolar-RWG discretizations of the EFIE. In Fig. 5(b), for the 0.1λ-square pyramid, this is the complete implementation, handling twice the number of edges as number of unknowns. In Fig. 6(b), for the 1λ-tetrahedron, an object with moderate electrical dimensions, the even-surface odd-volumetric implementation is hybrid, whereby the number of unknowns is reduced to the edges arising in the triangulation plus the edges matching the sharp edges of the object [6]. In view of these figures, the wedge testing shows improved RCS-accuracy in similar terms as the corresponding implementations with tetrahedral testing [6]. Similarly, the observed performance now with the even-surface odd-volumetric implementations is less dependent on the testing choices, conformal or nonconformal to the

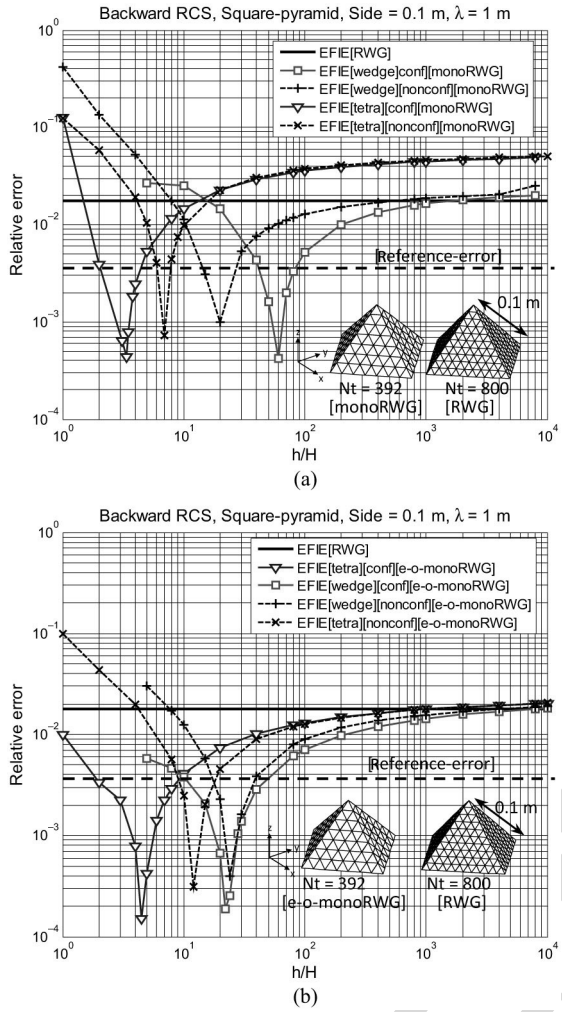

F5:1 Fig. 5. Relative error for a pyramid with square basis with side 0.1λ ($\lambda = 1$ m)
F5:2 of the backward scattered RCS versus the height H, defined as a fraction of the
F5:3 mesh parameter h, of the testing elements computed with several monopolar-
F5:4 RWG EFIE-implementations. (a) Volumetric. (b) Even-surface odd-volumetric.
F5:5 The meshes make use of 392 triangles for the monopolar-RWG and even-
F5:6 odd-monopolar-RWG discretizations; for the RWG-discretization, the mesh
F5:7 employs 800 triangles.

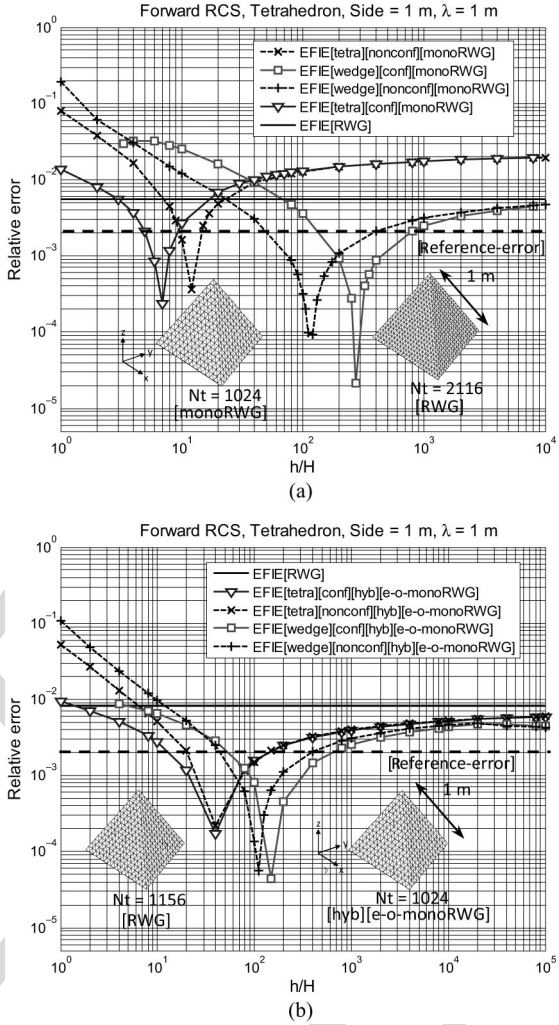

F6:1 Fig. 6. Relative error for a tetrahedron with side 1λ ($\lambda = 1$ m) of the for-
F6:2 ward scattered RCS versus the height H, defined as a fraction of the mesh
F6:3 parameter h, of the testing elements with several monopolar-RWG implemen-
F6:4 tations of the EFIE. (a) Volumetric. (b) Hybrid even-surface odd-volumetric.
F6:5 The meshes adopt 1024 triangles for the monopolar-RWG and hybrid even-
F6:6 odd-monopolarRWG discretizations; for the RWG-discretization, the meshes
F6:7 employ 2116 triangles in (a) and 1156 triangles in (b).

228 boundary surface, than their volumetric counterparts. Furthermore, the
229 H range with improved accuracy for the even-surface odd-volumetric
230 discretization with wedge testing is notoriously bigger than the ranges
231 observed for the volumetric discretization and same testing choice.
232 In particular, the H range with improved accuracy for EFIE[e-o-
233 monoRWG] and the square pyramid lies between h and $h/10^4$,
234 whereas for EFIE[hyb][e-o-monoRWG] and the tetrahedron, between
235 h and $h/10^5$. This involves at least two orders of magnitude bigger
236 than the observed H ranges for EFIE[wedge][monoRWG].
237 In Fig. 7, we plot, for the 0.1λ square pyramid, the near-field
238 relative error in terms of H and fixed degree of meshing for the
239 monopolar-RWG discretizations of the EFIE at a point inside the
240 object, at a distance of 0.02 m of the top vertex along the pyramid
241 axis. We define the near-field error as the ratio between the magnitudes
242 of the total and incident electric fields at that point [6]. As discussed
243 in detail in [6], the observed improved far-field accuracy prevails in
244 the near-field especially for electrically small objects. Indeed, in view
245 of Fig. 7, the best-performing H-values for each discretization are
246 consistent with the observed trends in Fig. 5 for the computed far-field.

B. Accuracy Versus N

247

248 In Figs. 8 and 9, we show for the square pyramid and the tetrahe-
249 dron, respectively, the relative error of the RCS computed with the
250 nonconforming EFIE-implementations with respect to reliable RCS
251 references against the number of unknowns. For each implementation
252 and object, we show two graphs corresponding to two H values that
253 are 10 and 100 times smaller than certain H values leading to the same
254 reference errors (see Figs. 5 and 6). For the square pyramid, this error
255 is 3.5e-3, whereas for the tetrahedron, it is 2e-3. In view of Figs. 5
256 and 6, for the volumetric implementations, the corresponding refer-
257 ence H-values are: 1) for the square pyramid, $h/42$ (wedge) and $h/2$
258 (tetrahedral) and 2) for the tetrahedron, $h/120$ (wedge) and $h/5$ (tetra-
259 hedral). Similarly, these H values for the even-surface odd-volumetric
260 implementations become: 1) for the square pyramid, $h/10$ (wedge)
261 and $h/2$ (tetrahedral) and 2) for the tetrahedron, $h/50$ (wedge) and
262 $h/13$ (tetrahedral).
263 The computed RCS over these ranges with the volumetric
264 monopolar-RWG discretization of the EFIE and wedge testing

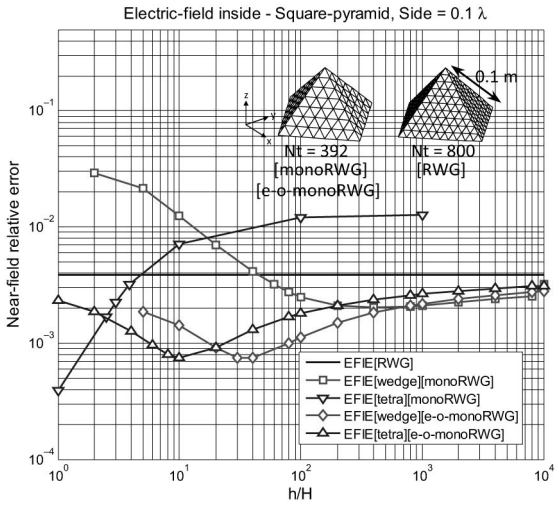

F7:1 Fig. 7. Near-field relative error inside the object versus the height H of the
F7:2 testing elements, with several monopolar-RWG EFIE-implementations for a
F7:3 square pyramid with side 0.1 m ($\lambda = 1$ m). The testing point is at distance
F7:4 of 0.02 m of the top vertex along the pyramid axis. The testing elements are
F7:5 defined conformal to the boundary surface.

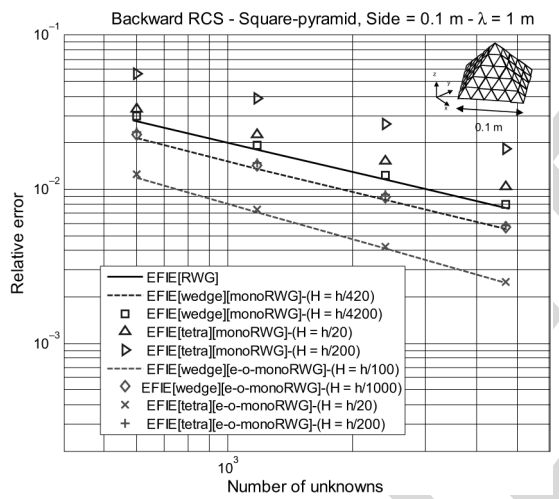

F8:1 Fig. 8. Relative error of the backward scattered RCS versus the number of
F8:2 unknowns computed with several monopolar-RWG EFIE-implementations for
F8:3 a square pyramid with side $= 0.1$ m ($\lambda = 1$ m). The testing elements are
F8:4 defined conformal to the boundary surface.

produces smaller error than the tetrahedral choice and the RWG-discretization (see Figs. 8 and 9). In contrast, the wedge and tetrahedral testing choices for the even-surface odd-volumetric monopolar-RWG discretization produce very similar performance, which is a sign of robustness. Moreover, the observed errors with the even-surface odd-volumetric implementations in both objects become much smaller than for the volumetric implementations.

C. Nonconformal Triangulations

In Fig. 10, we show the RCS for the composite object arising from the juxtaposition of a pyramid with rectangular basis on top of a rectangular prism. Two meshes are used: 1) a closed conformal mesh of 1920 triangles (mesh A) and 2) a nonconformal mesh of 832 triangles resulting from the interconnection of two independent open triangulations (mesh B). Neither the RWG-discretization

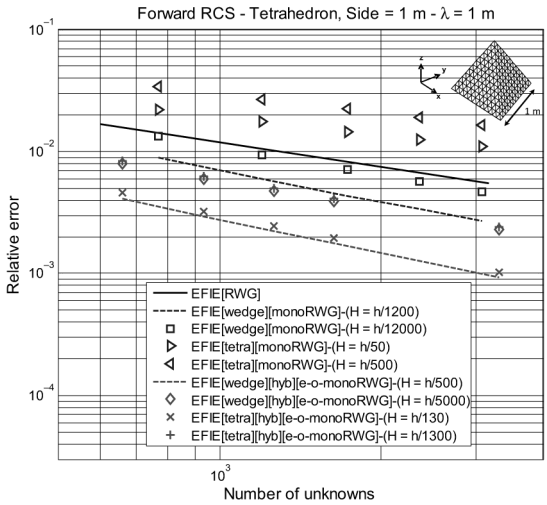

Fig. 9. Relative error of the forward scattered RCS versus the number of unknowns computed with several monopolar-RWG EFIE-implementations for a regular tetrahedron with side $= 1$ m ($\lambda = 1$ m). The testing elements are defined conformal to the boundary surface. F9:1 F9:2 F9:3 F9:4

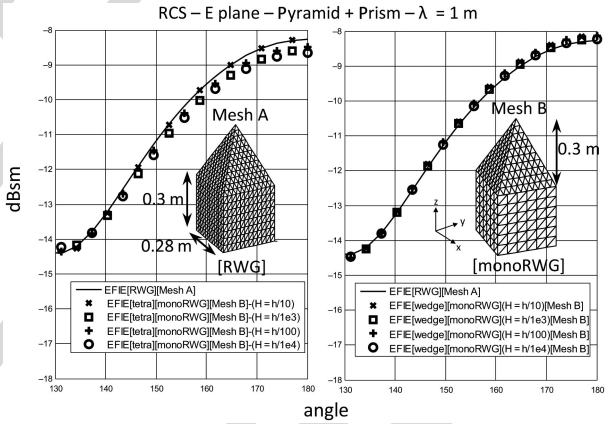

Fig. 10. xz plane cut of the RCS computed with several EFIE-implementations for an object composed of a pyramid on top of a rectangular prism. Meshes A and B employ, respectively, 1920 and 832 triangles. F10:1 F10:2 F10:3

nor the even-surface odd-volumetric monopolar-RWG discretization of the EFIE can handle the mesh B, where some neighboring triangles have nonmatching edges. Instead, the volumetric monopolar-RWG discretization, with the testing elements defined nonconformal to the boundary surface, stands for a flexible and versatile tool, well suited for the analysis of Mesh B. It is clear from Fig. 10 that the wedge testing in the volumetric monopolar-RWG discretization of the EFIE results in a more stable performance in terms of H than the tetrahedral testing.

V. Conclusion

The adoption of testing wedges conformal to the boundary surface in the volumetric monopolar-RWG discretization of the EFIE shows, for the sharp-edged conductors tested, improved accuracy for a wider range of heights of the testing elements than the choice of tetrahedral elements (between $h/10$ and $h/10^3$, for the moderately small objects tested, and between $h/10^2$ and $h/10^4$ for the 1λ-tetrahedron). For small enough heights, below one-hundredth of the mesh parameter, right triangular prisms, easy-to-implement, can be adopted too as successful testing elements. The even-surface odd-volumetric

monopolar-RWG discretization of the EFIE with wedge testing performs in a similar manner as described in [6] for tetrahedral testing elements. These implementations reach, for the sharp-edged conductors tested, much wider ranges of heights of the testing elements with improved accuracy (at least two orders of magnitude bigger than for the volumetric monopolar-RWG discretization and wedge testing).

For composite objects meshed with nonconformal triangulations where neighboring triangles have no matching edges, the volumetric monopolar-RWG discretization of the EFIE with testing over right triangular prisms appears as a more reliable option than the choice with tetrahedral testing because the computed RCS becomes more stable in terms of the heights of the testing elements. The even-surface odd-volumetric monopolar-RWG implementation, though, which assigns unknowns to the edges between pairs of adjacent facets, is not amenable in general to such triangulations.

We believe that the better suitability of the wedges as testing elements when compared with the tetrahedral elements lies in the fact that the wedge-monopolar testing functions enforce the null condition for the component of the inner electric field tangential to the boundary surface, which shows better consistency with the electric-field boundary condition at the surface.

REFERENCES

[1] S. M. Rao, D. R. Wilton, and A. W. Glisson, "Electromagnetic scattering by surfaces of arbitrary shape," *IEEE Trans. Antennas Propag.*, vol. 30, no. 3, pp. 409–418, May 1982.

[2] R. D. Graglia, D. R. Wilton, and A. F. Peterson, "Higher order interpolatory vector bases for computational electromagnetics," *IEEE Trans. Antennas Propag.*, vol. 45, no. 3, pp. 329–342, Mar. 1997.

[3] M. Carr, E. Topsakal, and J. L. Volakis, "A procedure for modeling material junctions in 3-D surface integral equation approaches," *IEEE Trans. Antennas Propag.*, vol. 52, no. 5, pp. 1374–1379, May 2004.

[4] P. Ylä-Oijala, M. Taskinen, and J. Sarvas, "Surface integral equation method for general composite metallic and dielectric structures with junctions," *Prog. Electromagn. Res.*, vol. 52, pp. 81–108, 2005.

[5] E. Ubeda, J. M. Rius, and A. Heldring, "Discretization of the EFIE in method of moments without continuity of the normal current component across edges," in *Proc. IEEE Antennas Propag. Soc. Int. Symp.*, Orlando, FL, USA, Jul. 7–13, 2013, pp. 448–449.

[6] E. Ubeda, J. M. Rius, and A. Heldring, "Nonconforming discretization of the electric-field integral equation for closed perfectly conducting objects," *IEEE Trans. Antennas Propag.*, vol. 62, no. 8, pp. 4171–4186, Aug. 2014.

[7] E. Ubeda and J. M. Rius, "Monopolar divergence-conforming and curl-conforming low-order basis functions for the electromagnetic scattering analysis," *Microw. Opt. Technol. Lett.*, vol. 46, no. 3, pp. 237–241, Aug. 2005.

[8] D. R. Wilton *et al.*, "Potential integrals for uniform and linear source distributions on polygonal and polyhedral domains," *IEEE Trans. Antennas Propag.*, vol. 32, no. 3, pp. 276–281, Mar. 1984.

[9] D. A. Dunavant, "High degree efficient symmetrical Gaussian quadrature rules for the triangle," *Int. J. Numer. Methods Eng.*, vol. 21, pp. 1129–1148, 1985.

[10] M. Gellert and R. Harbord, "Moderate degree cubature formulas for 3-D tetrahedral finite element approximations," *Commun. Appl. Numer. Methods*, vol. 7, pp. 487–495, 1991.

QUERY

Q1: Please check and confirm the inserted affiliation.